

# Thermal stress analysis of cordierite materials subjected to thermal shock

A. G. Tomba Martinez · M. A. Camerucci ·  
A. L. Cavalieri

Received: 9 November 2006 / Accepted: 24 January 2008 / Published online: 27 February 2008  
© Springer Science+Business Media, LLC 2008

**Abstract** Cordierite disks were obtained by slip casting and sintering at 1,450 °C for 2 h. Sintered disks were indented at the center of one flat surface. The fracture strength of indented disks was measured in biaxial flexure. The critical temperature differential was determined by sudden cooling of the center of the indented surface at high temperature, using a high-velocity air jet at room temperature. The initial temperature was successively increased by 10 °C until crack propagation was detected with the naked eye. Temperature and stress distributions during air impinging were calculated by a finite element analysis. The heat transfer coefficient was estimated by fitting experimental temperature profiles. A radial variation of the coefficient that considers its increment beyond the stagnation region and a diminution toward the disk periphery was assumed. The calculated cordierite thermal stresses were analysed in relation to experimental data. Also, the comparison with alumina tested in similar conditions was included.

## Introduction

The conventional use of cordierite ( $2\text{MgO}\cdot 2\text{Al}_2\text{O}_3\cdot 5\text{SiO}_2$ ) and cordierite-based ceramics in fast-cycle heating furnaces is due to their high thermal shock resistance. In addition, they have attracted attention for use as substrate materials in high-performance systems in replacement of conventionally used alumina materials. Several studies

about the mechanical behavior of cordierite materials have been published [1–3], while limited data on thermal shock response are available [4].

The practical significance of studying the thermal shock behavior of ceramics is associated with the great complexity of the material degradation under these conditions. Therefore, there is not a unique and simple thermal shock test that yields quantitative and easily extrapolatable results. The data are closely linked to the experimental conditions and their analysis cannot be done abstracting the experimental aspects. The actual thermal stress undergone by the specimen must be known to achieve an insight into this complex behavior. This can be accomplished by the calculation of the stresses arising during the thermal shock by the application of numerical models that attempt to simulate the thermomechanical conditions with minor simplifications.

Assuming that the material response to mechanical and thermomechanical loadings is equivalent, the higher the amount of information about the mechanical behavior of a material, the deeper the insight of its response under thermal shock conditions.

This work covers the numerical calculation of the thermal stresses generated in cordierite disks subjected to thermal shock tests. A comparative analysis is performed with cordierite subjected to mechanical stresses, and alumina tested in similar conditions [5–8].

## Materials and methods

### Preparation and characterization of specimens

Disks of  $17.50 \pm 0.02$  mm in radius and  $2.67 \pm 0.01$  mm in height were fabricated by slip casting an aqueous

A. G. Tomba Martinez (✉) · M. A. Camerucci · A. L. Cavalieri  
Instituto de Investigaciones en Ciencia y Tecnología de  
Materiales (INTEMA), Facultad de Ingeniería, Universidad  
Nacional de Mar del Plata, CONICET, Av. J. B. Justo 4302,  
Mar del Plata 7600, Argentina  
e-mail: agtomba@fi.mdp.edu.ar

suspension of a commercial cordierite powder (CORCR Baikowski; mean particle diameter,  $D_{50} = 2.1 \mu\text{m}$ ; specific surface,  $S_{\text{S BET}} = 2.5 \text{ m}^2 \text{ g}^{-1}$ ; pycnometric density,  $\delta_{\text{PIC as-received cordierite}} = 2.60 \text{ g cm}^{-3}$ ) [9]. The composition of the starting powder (impurities  $< 0.17 \text{ wt.}\%$ ) is shifted toward the alumina corner in the  $\text{Al}_2\text{O}_3\text{--SiO}_2\text{--MgO}$  phase equilibrium diagram with respect to stoichiometric cordierite [10]. Cordierite, and mullite as a secondary phase, were identified by XRD analysis [10]. Green samples were ground with SiC (320 and 600 grit) to adjust their dimensions and achieve plane-surfaces parallelism.

The disks were sintered at  $1,450 \text{ }^\circ\text{C}$  (heating and cooling rates of  $1 \text{ }^\circ\text{C min}^{-1}$ ) for 2 h in an electric furnace with  $\text{MoSi}_2$  heating elements. Temperatures were measured using a Pt-30%Rh/ Pt-6%Rh thermocouple (accuracy  $\pm 2 \text{ }^\circ\text{C}$ ).

An average densification degree ( $\% \delta_{\text{SINT}}/\delta_{\text{PIC cordierite at } 1450 \text{ }^\circ\text{C}}$ ) of 97.3% was calculated considering the sintered disk density ( $\delta_{\text{SINT}}$ ) determined by Archimedes method in water, and the density of calcined powder at  $1,450 \text{ }^\circ\text{C}$ , 2 h, was measured by pycnometry ( $\delta_{\text{PIC cordierite at } 1,450 \text{ }^\circ\text{C}} = 2.57 \text{ g cm}^{-3}$ ) [9, 10]. The phases developed at the sintering temperature identified by XRD and FTIR techniques were cordierite, mullite, and glass (84, 10, and 6 wt.%, respectively) [9].

A homogeneous microstructure with mainly equiaxed cordierite and mullite grains of similar submicron mean size ( $\approx 0.5 \mu\text{m}$ ) was observed by SEM (Philips 505) [9, 10]. In addition, only a few elongated grains (aspect ratio  $\approx 1.9$ ) attributed to mullite grown in the presence of a liquid phase were observed (located at triple points and grain boundaries), intergranular pores ( $< 10 \mu\text{m}$ ) homogeneously distributed, along with a few isolated pores up to  $40 \mu\text{m}$ .

The sintered disks were indented at the center of one of their plane surfaces (Tukon 300 microhardness tester, Vickers indenter, 44.1 N, 15 s) to introduce a controlled critical defect due to an equipment limitation (maximum furnace temperature). Four well-developed median-radial cracks arose from the corners of the indentation (crack semidiagonal:  $46 \mu\text{m}$ ; crack semilength plus crack semidiagonal:  $152 \pm 17 \mu\text{m}$ ).

### Mechanical test

The fracture strength of the indented disks was evaluated in biaxial flexure. A loading ball (diameter:  $8.04 \pm 0.02 \text{ mm}$ ) on a discontinuous ring (12 balls in contact; ring diameter:  $19.50 \pm 0.1 \text{ mm}$ ) fixture [11–13] was employed. A uniform biaxial stress field at the center of the flexured surface was generated. Having in mind that the radius of the uniform stress region is about one-third of the disk height [13], the size of the indentation defect resulted in being about six

times smaller than this radius. An Instron testing machine model 8501 with displacement control ( $0.05 \text{ mm min}^{-1}$ ) was employed.

### Thermal shock test [11]

Each disk was mounted horizontally on refractory material in an electric furnace (Kanthal heating elements), with the indented surface upward. The disk equilibrated at a high temperature ( $T_i$ ) was suddenly cooled using a high-velocity air jet ( $330 \text{ ms}^{-1}$ ) at room temperature ( $T_0 = 27 \text{ }^\circ\text{C}$ ) onto the center of the indented surface for 20 s. The air was channelled using a silica tube (inner radius:  $3.58 \pm 0.02 \text{ mm}$ ) placed at  $90^\circ$  to, and 3 mm above, the surface.

Each specimen was tested by successively increasing  $T_i$  by  $10 \text{ }^\circ\text{C}$  until crack propagation was detected with the naked eye after cooling. The thermal shock resistance was evaluated as  $\Delta T_C = T_C - T_0$ , where  $T_C$  is the critical temperature defined as the value of  $T_i$  at which cracks were detected (initiation condition).

During the air impingement, the temperature of the disk at two points on its bottom surface—at the center, and at  $14.5 \pm 0.02 \text{ mm}$  from it—were recorded by attaching fast-response Pt-10%Rh/Pt thermocouples (accuracy  $\pm 0.25\%$ ). Only when cracks were detected, the  $T$  versus  $t$  (time) recording at the disk center exhibited a slight although visible change in the rate of temperature decrease. The time at which this event occurred was estimated as the experimental fracture time ( $t_f$ ).

The aspect of both the cracks and the fracture surfaces was studied by ocular inspection and SEM, respectively.

### Numerical calculation of temperature and stress distributions

The temporal and spatial distributions of temperature and stress in the specimen subjected to thermal shock were calculated by a finite element method using a commercial code (LUSAS) and thermomechanical semi-coupled analysis. Because of the axial symmetry of the problem, only the transverse half-plane of the disk and the refractory material was simulated as a bidimensional axisymmetric problem. The mesh was regular with 576 parabolic square elements, and a higher discretization in the jet radius region was used (element length in this region was 4.4 times smaller than the element length at a farther distance). Cartesian coordinates were used for the calculus in the mesh domain, the  $x$ -axis being the radial and the  $y$ -axis parallel to the direction of disk height (see Fig. 4). The values of cordierite and refractory material properties were taken from literature [1, 3, 14–16] (Table 1).

The simulation model considered an imposed air flow over the upper surface of the disk. The convective heat

**Table 1** Values of cordierite and refractory material properties

	$k$ (W °C <sup>-1</sup> m <sup>-1</sup> )	$C_p$ (J kg <sup>-1</sup> °C <sup>-1</sup> )	$\delta$ (kg m <sup>-3</sup> )	$\alpha$ (1 °C <sup>-1</sup> )	$\nu$	$E$ (GPa)
Cordierite [1, 3, 14, 15]	3.34	720	2,600	$2.4 \times 10^{-6}$	0.28	135
Refractory material [16]	1.50	960	2,050	$6.0 \times 10^{-6}$	0.14	400

$k$ : Thermal conductivity;  $C_p$ : Heat capacity;  $\delta$ : Density;  $\alpha$ : Average linear thermal expansion coefficient (20–900 °C);  $\nu$ : Poisson modulus;  $E$ : Young modulus

transfer coefficient ( $h$ ) was assumed invariant with the temperature. Its radial variation was simulated considering: (a) an increment of  $h$  beyond the stagnation region [17, 18] and (b) a diminution of  $h$  toward the disk periphery, according to:

$$h(x) = h_0 \quad x \leq r_0$$

$$h(x) = \frac{h_0}{x} r_0 \quad r_0 < x \leq r_c$$

$$h(x) = \frac{h'_0}{x} r_0 \quad r_c < x \leq R$$

where  $r_0$  and  $R$  are the jet and the disk radii, respectively,  $r_c$  is the value of the radius from which the behavior of the convective coefficient changes and  $h_0$  is the value of  $h$  in the impinging jet region. The magnitudes of  $h_0$ ,  $h'_0$  and  $r_c$  were estimated using a previously designed methodology [11, 19]. It implies the fitting of temperature profiles calculated by FEA at the center and at the periphery of the bottom disk surface with the corresponding experimental profiles. Values of  $h_0$ ,  $h'_0$ , and  $r_c$ , were used as fitting parameters. For each  $T_i$ , the experimental temperature profiles at each point were the average of the thermal recordings for every tested disk at this  $T_i$ . Assuming that  $r_c$  is just a function of geometric factors and air flow characteristics, a value of  $4.74 \pm 0.65$  mm determined for alumina [11, 19] was used. The errors of  $h_0$  and  $h'_0$ , estimated taking the temperature profile for each disk at  $T_i$  as a replica, were 24% and 3%, respectively.

Heat transfer by conduction due to the contact between the disk and the refractory support was considered (conductance  $\approx 10^3$  W m<sup>-2</sup> °C<sup>-1</sup> [11, 19]). No radiation effects were taken into account. Remaining boundaries were assumed to be adiabatic.

For the stress evolution, an axisymmetric deformation problem was considered. Both cordierite and the refractory support were assumed as elastic, linear, and isotropic materials. The radial displacements for the nodes located on the central axis in the cordierite disk, as well as in the refractory support, were constrained.

## Results and discussion

### Experimental supporting data

Thermal shock and mechanical testing data of indented cordierite disks have been previously reported [9]. Mechanical resistance ( $\sigma_F$ ) of  $49.5 \pm 13.8$  MPa and a Weibull modulus of 4.2 were obtained for indented cordierite disks at room temperature [9]. The thermal shock data are summarized in Table 2, together with the magnitude of parameter  $R'$  calculated with values from Table 1 and the mean value of  $\sigma_F$ .

Figure 1 shows the typical crack pattern of indented cordierite disks broken in thermal shock tests. For comparative purposes, a disk fractured in biaxial flexure test is also shown.

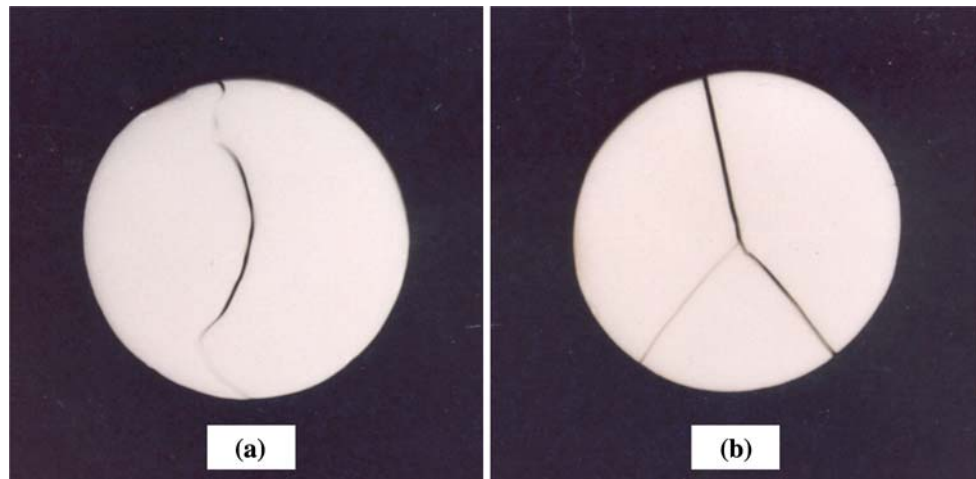
Experimental data for machined (SiC, 320 grit) alumina disks tested in similar mechanical and thermal shock conditions, have also been previously reported [5, 8]. A mechanical strength of  $220 \pm 38$  MPa and a Weibull modulus of 6.9 were determined. Thermal shock data are reported in Table 2. The  $R'$  parameter for alumina (Table 2) was calculated using the mean  $\sigma_F$  values and other thermal and mechanical properties extracted from literature [5]. According to the value of  $R'$  calculated for

**Table 2** Previous thermal shock data

	$\Delta T_C$ (°C)	$R'$ (W m <sup>-1</sup> )	$t_f$ (s)	Fracture	
				Crack pattern	Origin
Cordierite [9]	$970 \pm 91$	380	5–10	Radial, crossing the thickness, tortuous, without branching. Low fragmentation (2–3 parts).	Indentation flaw
Alumina [5, 7, 8]	$916 \pm 54$	450	3–5	Radials and circulars, crossing the thickness, tortuous. High fragmentation (3–7 parts).	Machining flaw

$R' = [k\sigma_F(I - \nu)/E\alpha]$ : thermal shock resistance parameter;  $t_f$ : fracture time

**Fig. 1** Crack patterns of cordierite disks broken in thermal shock test (a) and biaxial flexure (b)



alumina and cordierite materials, a higher resistance to thermal shock should be expected for the former.

#### Numerical calculation

##### Temperature distributions

Three representative  $T_i$  were selected to obtain  $h$ , covering the complete range of used temperatures: 870, 970, and 1,070 °C. The values of  $h_0$  and  $h_0'$  for tested cordierite disks are reported in Table 3 together with those obtained for alumina [6, 7]. Figure 2 shows experimental temperature profiles (at the center and at the periphery of the bottom surface) together with the fitted curves for each  $T_i$ . Similar decreasing curves were obtained in alumina although the difference in temperature between the peripheral point and the center was always higher than that of cordierite (regardless of time and  $T_i$ ).

In general, the values of  $h$  for cordierite were lower than those for alumina. Since the convective heat transfer coefficient depends on multiple variables [20], such as the type of solid material and its surface characteristics (roughness, for instance), it was difficult to account for the observed tendency. The relative magnitude of cordierite and alumina values of  $h$  would be a factor, among others, that could explain the higher thermal shock resistance of the former, which is not predicted by  $R'$  values [9]

**Table 3** Fitting parameters

	$T_i$ (°C)	$h_0$ (W m <sup>-2</sup> °C <sup>-1</sup> )	$h_0'$ (W m <sup>-2</sup> °C <sup>-1</sup> )
Cordierite	870	130	780
	970	100	630
	1,070	100	630
Alumina [7]	870	160	650
	920	180	650
	980	200	650

(Table 2). This fact highlights the restrictions of the last parameter, which does not consider the microstructure nor the convective heat transfer conditions.

The dependence of cordierite's  $h$  coefficient with  $T_i$  is not clear. Moreover, it seemed to be opposite to alumina. In this case, the observed increment of the heat transfer coefficient with  $T_i$  was partially explained taking into account the increase of air thermal conductivity with temperature [11], which could also occur in cordierite. It is possible that the dependency on temperature of the material properties used in the numerical calculation would clarify the thermal behavior of  $h$  in cordierite. However, in spite of this issue, the fitting quality (Fig. 2) lends support to the use of estimated  $h$  values in the temperature and stress calculations.

The spatial temperature distributions of cordierite for every  $T_i$  exhibited the same characteristics as those of alumina. The lowest temperatures were registered at the

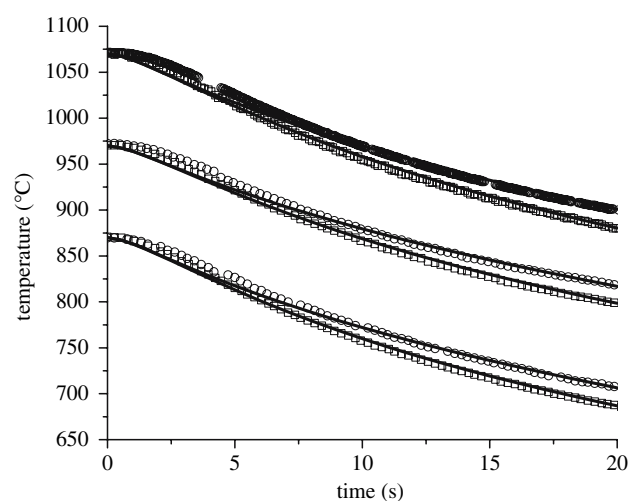


**Fig. 2** Experimental temperature profiles of cordierite disks at central point (●) and peripheral point (○), together with the corresponding fitting curves (—)

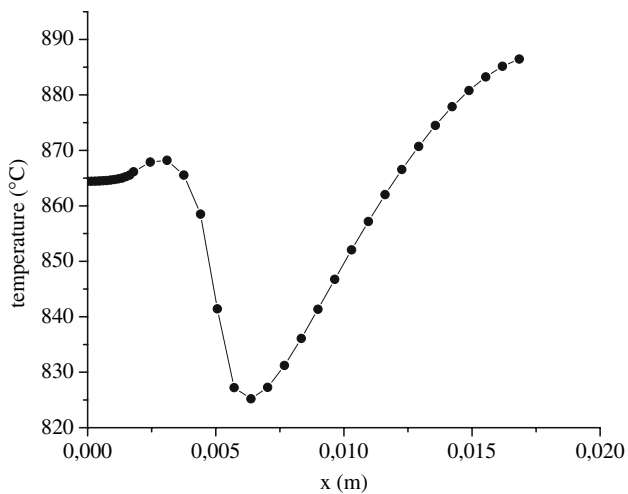


**Fig. 3** Radial temperature distribution on the upper surface of cordierite disk ( $T_i = 970$  °C, 6 s from the cooling onset)

disks' upper surface, where the air impinged, in both materials. Figure 3 shows the radial distribution of temperature for  $T_i = 970$  °C on the upper surface of the disk after 6 s, where typical maxima and minima values were observed in relation to the considered radial variation of  $h$ . The temperature drop at the center of cordierite disks was notably less than that of the other local minimum.

Similar thermal profiles were also obtained in alumina, although the positions where the local minima and maximum occurred were displaced toward the center. Converse to cordierite, in alumina disks the cooling of the center was rather pronounced and similar to that of the other local minimum. This difference in thermal distributions was in agreement with the respective heat transfer coefficients.

#### Stress distributions

Figure 4 shows the contour plot of the radial ( $\sigma_x$ ) and tangential ( $\sigma_z$ ) components of the stress after 6 s from the beginning of the air impingement (around the average experimental fracture time) for 970 °C. Similar plots were obtained for other times and  $T_i$ .

In the beginning spatial stress distribution resulted qualitatively similar to that calculated for alumina. At the upper surface, local minima and maxima in  $\sigma_x$  and  $\sigma_z$  were obtained as a consequence of temperature variations. The position of the maximum tensile stress between 5 and 10 s, in the range of experimental fracture times, always occurred in the tangential component at  $x_M = 5.72$  mm. Conversely, in alumina, the maximum tensile stress value was developed at the center, where  $\sigma_x = \sigma_z$ , or at 5.72 mm in the  $\sigma_z$  component. Both behaviours are explained by the temperature minima in the thermal distributions.

In Fig. 5,  $\sigma_x$  and  $\sigma_z$  variation along the upper surface, after 6 s from the beginning of the thermal shock, for

$T_i = 970$  °C, are shown. The curves were similar to those obtained for other times and  $T_i$ . Both components of stress, radial and tangential, changed in a way similar to those calculated for alumina. Values of  $\sigma_x$  were close to  $\sigma_z$  up to  $x \sim 4$  mm in cordierite, while this similarity extended to  $x \sim 2$  mm in alumina.

The crack patterns observed for cordierite (Fig. 1) and alumina disks [5, 8] were consistent with an equibiaxial stress distribution. Radial and/or circular cracks in the impingement region of alumina disks [5, 8] were associated with the position of maxima tensile stresses, since the fracture randomly originated at processing flaws [8]. The failure of cordierite disks initiated at the indentation [9], and although the crack propagation began in a radial manner, it then deflected tangentially near the disk periphery (Fig. 1). The features of the crack path are explained by the presence of radial indentation cracks, the highest tangential stress level up to  $\sim 8$  mm, and the further increment of  $\sigma_x$  above  $\sigma_z$  beyond this radial position (which accounted for the crack deviation near the disk periphery).

Figure 6 shows the temporal evolution of the stress components in cordierite disks at the center and at  $x_M$  for 970 °C. Similar curves were obtained for other  $T_i$ . The profiles seemed to be those of alumina, although remarkable differences were observed between the stress levels and the times at which the maxima values were reached. In Table 4 the maximum tensile stresses are reported together with the times at which they are reached. Maximum stresses for cordierite were 5–10 times lower than those for alumina, in agreement with the lower value of the heat transfer coefficient in the former. Other factors could also have contributed to this difference, mainly the lower thermal expansion coefficient of cordierite (Table 1). The relative magnitudes of maximum tensile stress in cordierite and alumina subjected to similar  $\Delta T$  explain the higher experimental thermal shock resistance of the former, since the severity of the quenching turns out to be lower in cordierite.

The magnitude of the stress components for cordierite material (Table 4) was practically independent of the temperature, while in alumina the stresses increased with  $T_i$ . As was mentioned earlier for the thermal dependence of  $h$ , it would be possible to clarify the dependency of stresses values with the temperature if the thermal variation of cordierite properties is considered in the numerical model. This assumption of thermal independence of properties could also explain the difference between the experimental fracture time in cordierite and those in which the highest tensile stresses occurred (calculated fracture time). Conversely, in alumina both experimental and calculated fracture times agreed satisfactorily. One cannot discard the fact that the experimental fracture time for cordierite could

**Fig. 4** Contour plots of radial ( $\sigma_x$ ) and tangential ( $\sigma_z$ ) stress components of cordierite disk ( $T_i = 970$  °C, 6 s from the cooling onset)

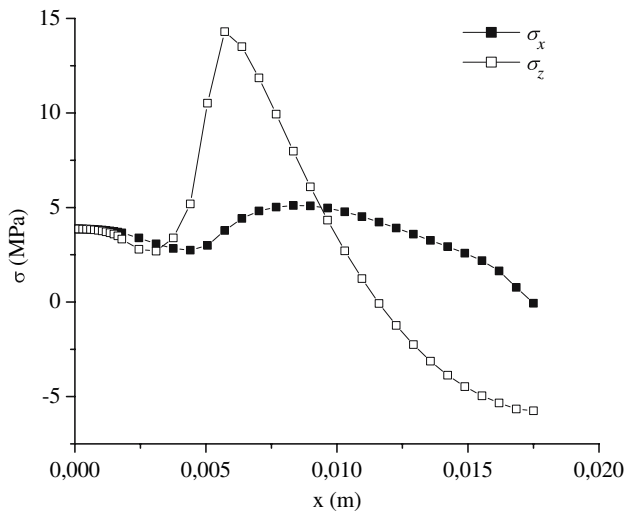
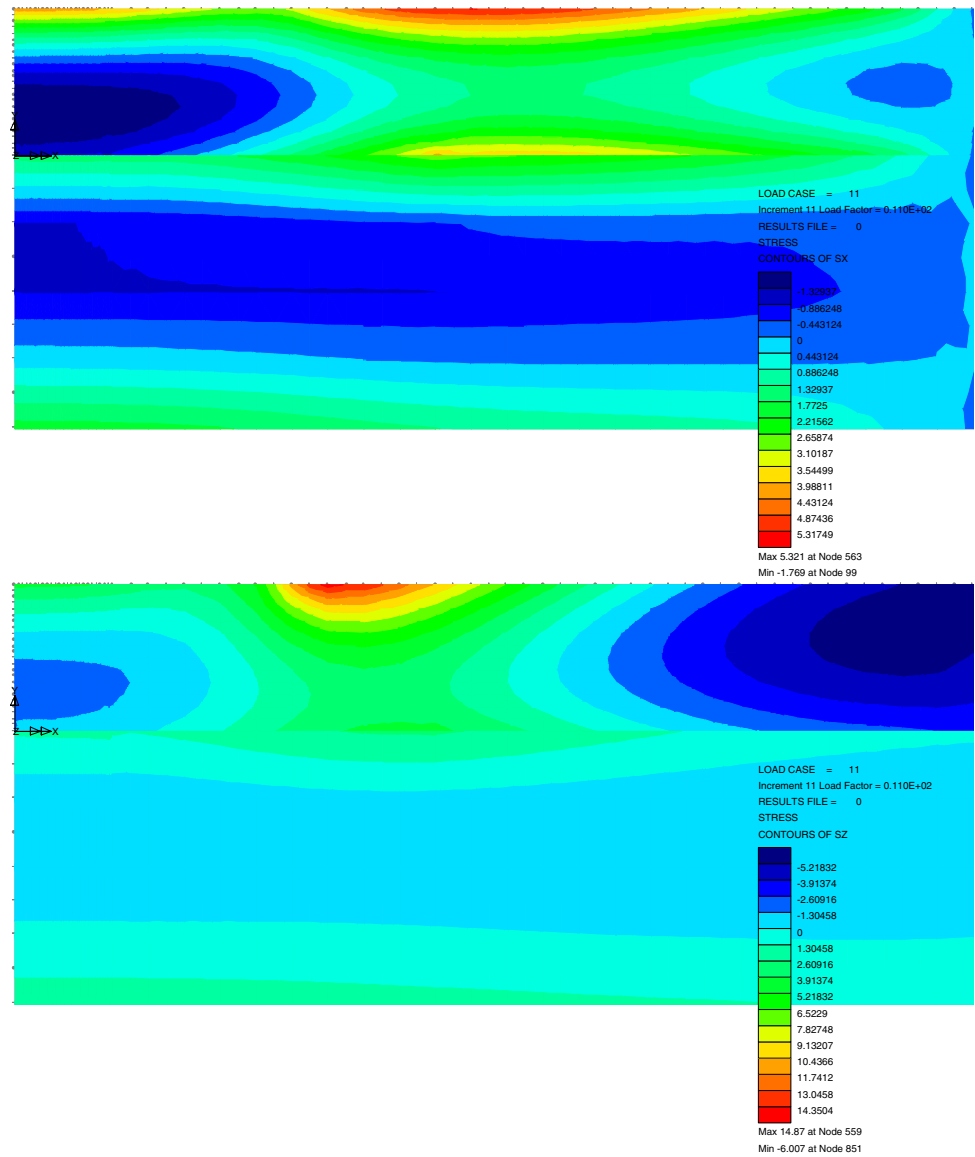


**Fig. 5** Radial variation of stress on the upper surface of cordierite disk ( $T_i = 970$  °C, 6 s from the cooling onset)

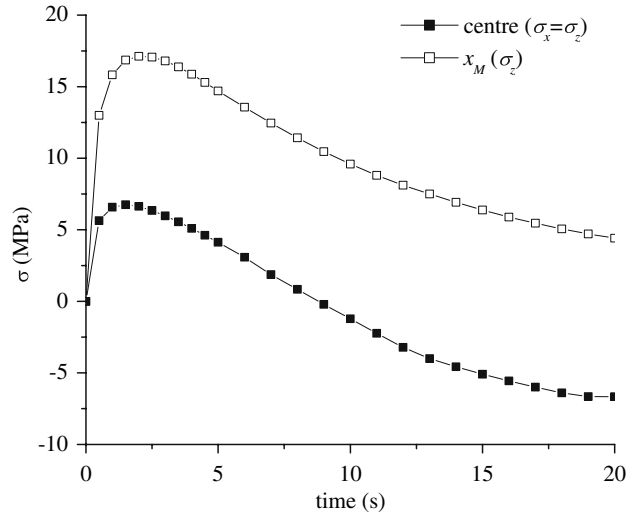


**Fig. 6** Temporal evolution of stress components at points on the upper surface of cordierite disk ( $T_i = 970$  °C)

**Table 4** Maximum values of tensile stresses

	$T_i$ (°C)	Centre		$x_M = 5.72$ mm	
		$\sigma_x = \sigma_z$ (MPa)	Time (s)	$\sigma_z$ (MPa)	Time (s)
Cordierite	870	7.8	1.5	18.5	2.0
	970	6.7	1.5	17.1	2.0
	1,070	7.6	1.5	19.0	2.0
Alumina [7]	870	52.0	6.1	77.0	3.6
	920	64.0	5.5	81.5	3.0
	980	83.2	7.0	89.0	3.4

be overestimated to a higher degree than that for alumina material due to its lower thermal conductivity (about a half that of alumina).

Taking into account phenomenological aspects of fracture, differences between cordierite and alumina in the stress analyses must be established. In the former, the defect introduced by indentation acted as the fracture origin whether in conjunction with the microstructure or not, as was confirmed by fractography [9]. Therefore, the stress at the disk center determined the thermal failure, in spite of the calculated maximum tensile stress occurring at  $x = 5.72$  mm. In alumina, the situation was different because the fracture was initiated at randomly distributed machining flaws, and cracking could have originated anywhere in the region of high stress levels ( $\sim 5$  mm in radius [7]).

In general, it is assumed that for equivalent stress distributions, the fracture by thermal stresses is produced at the same critical tensile stress that occurs under mechanical loading. In cordierite, the fracture stress measured by biaxial flexure ( $\sigma_F = 49.5 \pm 13.8$  MPa) resulted notably higher in comparison with the maximum thermal tensile stress at the disk center (Table 4). A similar difference was determined in alumina and it was attributed to the combination of several factors [6, 7]. Two of them, the dependence of mechanical strength on temperature and the restrictions of the numerical model, also apply to cordierite. In addition, other factors could contribute to increase the discrepancy between mechanical and thermal fracture stresses in indented cordierite disks.

The calculated thermal stresses in indented cordierite disks may be underestimated by the simplifications of the actual thermal shock conditions assumed in the numerical model. On one hand, the dependence of material properties on temperature was neglected in the finite element analysis and its consideration could give more realistic values of stresses. On the other hand, the effect of the indentation on the stress profiles was not considered in the numerical simulation. The presence of the indentation modifies the stress distribution because of: (a) the local variation of  $h$

coefficient that could alter the temperature distribution and (b) the residual stress field that is generated around it [21, 22].

Furthermore, one cannot discard the possibility that the failure of indented cordierite disks in thermal shock conditions actually occurred at a lower level of stress in comparison to critical stress in mechanical loading. The effect of successive heating on the indentation residual stress field (inferred from the difference in flaw size in disks tested mechanically at room temperature and under thermal shock [9, 23]) and on the characteristics of the indentation crack tip (blunting) could modify the fracture behavior of the material under thermal shock with respect to its response to mechanical stresses.

### Critical assessment

As a first approach to a very complex problem, the numerical model used, although limited, correctly predicted the features of the fracture induced by thermal stresses on cordierite materials.

However, it is expected that a more sophisticated numerical model of indented cordierite under thermal shock could give thermal and stress distributions closer to the actual ones. Possible improvements may be made by considering the thermal dependence of the material properties and the heat transfer coefficient, and the effect of the indentation in temperature and stress fields.

In addition, to compare the calculated thermal and mechanical stresses, measurements of the latter at high temperature and the effect of temperature on indentation cracks under thermal shock conditions should be also considered.

### References

1. Monroe DL, Wachtman JB Jr (1989) The mechanical properties of cordierite-mullite composites as a function of temperature. In: Proc. 1st Conf. of the European Ceram. Soc., Elsevier Applied Science, Amsterdam, p 18
2. Suzuki H, Ota K, Saito H (1988) J Mater Sci 23:1534. doi: [10.1007/BF01115687](https://doi.org/10.1007/BF01115687)
3. Anderson RM, Gerhardt R, Wachtman JB Jr (1989) Adv Ceram 26:265
4. Suzuki H, Saito H (1992) J Eur Ceram Soc 9:365
5. Tomba Martinez AG, Cavalieri AL (2000) J Eur Ceram Soc 20:889
6. Tomba Martinez AG, Cavalieri AL (2001) Mater Res Bull 4:7
7. Tomba Martinez AG, Cavalieri AL (2001) J Eur Ceram Soc 21:1205
8. Tomba Martinez AG, Cavalieri AL (2002) J Am Ceram Soc 85:921
9. Tomba Martinez AG, Camerucci MA, Urretavizcaya G, Cavalieri AL (2002) Br Ceram Trans 101:94
10. Camerucci MA, Urretavizcaya G, Cavalieri AL (2001) J Eur Ceram Soc 21:1195

11. Tomba Martinez AG (1998) Thermal shock of dense alumina. Ph.D. Thesis, Universidad Nacional Mar del Plata, Argentina
12. Wachtman JB, Capps W, Mandel J (1972) *J Mater* 7:188
13. Shetty DK, Rosenfield AR, McGuire P, Bansal GK, Duckworth WH (1980) *Ceram Bull* 59:1193
14. Mussler BH, Shafer MW (1984) *Ceram Bull* 63:705
15. Camerucci MA, Urretavizcaya G, Castro MS, Cavalieri AL (2001) *J Eur Ceram Soc* 21:2917
16. Fisher RE (1988) Advances in refractories technology. *Ceram Trans* 4; The American Ceramic Society, Westerville
17. Poulson B (1983) *Corros Sci* 23:391
18. Cooper D, Jackson DC, Launder BE, Liao GX (1993) *Int J Heat Mass Transfer* 36:2675
19. Tomba Martinez AG, Cavalieri AL (2000) *Mater Sci Eng A* 276:76
20. Kreith F (1977) *Principios de transferencia de calor*, Herrero Hermanos Sucesores, S.A., México
21. Osterstock F, Monot I, Desgardin G, Mordike BL (1996) *J Eur Ceram Soc* 16:687
22. Leoni M, Scardi P, Sglavo M (1998) *J Eur Ceram Soc* 18:1663
23. Tomba Martinez AG, Camerucci MA, Cavalieri AL (2005) *J Eur Ceram Soc* 26:2527